Cell Host & Microbe
Article

Salmonella Gut Invasion Involves TTSS-2-Dependent Epithelial Traversal, Basolateral Exit, and Uptake by Epithelium-Sampling Lamina Propria Phagocytes

Andreas J. Müller,[1,5] Patrick Kaiser,[1,5] Kurt E.J. Dittmar,[2,5] Thomas C. Weber,[1] Sabine Haueter,[1] Kathrin Endt,[1] Pascal Songhet,[1] Christa Zellweger,[1] Marcus Kremer,[3] Hans-Jörg Fehling,[4] and Wolf-Dietrich Hardt[1,*]
[1]Institute of Microbiology, D-BIOL, ETH Zürich, 8093 Zürich, Switzerland
[2]Helmholtz Center for Infection, 38124 Braunschweig, Germany
[3]Städtisches Klinikum München, 80337 München, Germany
[4]Institute of Immunology, University Clinics Ulm, 89081 Ulm, Germany
[5]These authors contributed equally to this work
*Correspondence: hardt@micro.biol.ethz.ch
DOI 10.1016/j.chom.2011.11.013

SUMMARY

Salmonella Typhimurium causes diarrhea by infecting the epithelium and lamina propria of the intestinal mucosa and by secreting various effector proteins through type III secretion systems (TTSSs). However, the mechanisms by which _Salmonella_ transverses the epithelium and is subsequently released into the lamina propria are poorly understood. Using a murine _Salmonella_-diarrhea model and in vivo microscopy, we show that epithelial traversal requires TTSS-1-mediated invasion and TTSS-2-dependent trafficking to the basolateral side. After being released into the lamina propria, the bacterium is transiently extracellular before being taken up by phagocytes, including $CD11c^{+}CX_3CR1^{high}$ monocytic phagocytes (MPs), which were found to constitutively sample cellular material shed from the basolateral side of the epithelium. Thus, _Salmonella_ infects the cecal mucsa through a step-wise process wherein the bacterium transverses the epithelium through TTSS-2-dependent trafficking and then likely exploits lamina propria MPs, which are sampling the epithelium, to enter and replicate within the host.

INTRODUCTION

The mammalian intestine is a site of intimate coexistence of the host organism with microbes (Macpherson and Harris, 2004). Maintenance of health depends on barrier functions and immune defenses limiting microbial access to the gut tissue. Enteropathogenic bacteria have evolved strategies for breaching these defenses. However, at the mechanistic level these strategies are still not well understood.

Salmonella enterica subspecies I serovar Typhimurium (*S.* Typhimurium) is a frequent cause of diarrhea and serves as a model for studying the subversion of mucosal defenses by bacterial pathogens (Kaiser et al., 2012). After oral ingestion, *S.* Typhimurium infects the gut tissue, triggers mucosal inflammation, and reaches the mesenteric lymph nodes. In immunocompromised patients as well as in murine models, spread to systemic sites such as liver and spleen is also observed (Hapfelmeier et al., 2004; Reddy et al., 2010; Santos and Bäumler, 2004; Takeuchi, 1967).

Breaching the epithelial barrier is thought to be the initial step of the *S.* Typhimurium infection. Experimental evidence suggests that the pathogen may engage different mechanisms for breaching the epithelial barrier at different sites of the intestine (Figure 1A). In the terminal ileum of mice, the pathogen may cross the epithelium in a one-step process. Here, $CD11c^{+}CX_3CR1^{high}$ lamina propria monocytic phagocytes (termed CX_3CR1^{high} MΦ in this paper) were shown to extend thin, arm-like protrusions across the epithelium and thereby facilitate pathogen transport from the gut lumen into the lamina propria (Chieppa et al., 2006; Niess et al., 2005). Paracellular penetration might represent an alternative one-step mechanism for breaching the epithelial barrier (Köhler et al., 2007). In contrast, *S.* Typhimurium invasion into the Peyer's patches of the small intestine occurs in two steps via specialized M cells. Uptake by M cells is followed by the release into the underlying dome region (Figure 1A) (Hase et al., 2009; Santos and Bäumler, 2004). Finally, *S.* Typhimurium can employ virulence factors such as type III secretion systems (TTSSs) for the two-step invasion of the absorptive mucosa. The first step, i.e., epithelial invasion, has been well studied in tissue culture and animal models (Frost et al., 1997; Reis et al., 2003; Santos et al., 2002; Takeuchi, 1967). In a subsequent step, the pathogen reaches the lamina propria. However, the nature of the second step, i.e., the mechanisms driving pathogen traffic to the basolateral side and the way the pathogen exits into the lamina propria, had remained unclear.

The streptomycin mouse model for *S.* Typhimurium diarrhea allows detailed mechanistic studies (Kaiser et al., 2012). In this model, pathogen invasion and massive mucosal inflammation occurs in the absorptive mucosa of the cecum and colon (Barthel et al., 2003; Coburn et al., 2005; Hapfelmeier et al., 2008; Hapfelmeier et al., 2005; Müller et al., 2009). Pathogen-derived virulence factors, namely TTSS-1, facilitate invasion into enterocytes and the lamina propria (Hapfelmeier et al., 2004; Müller et al., 2009). Also, it is well established that the pathogen is present

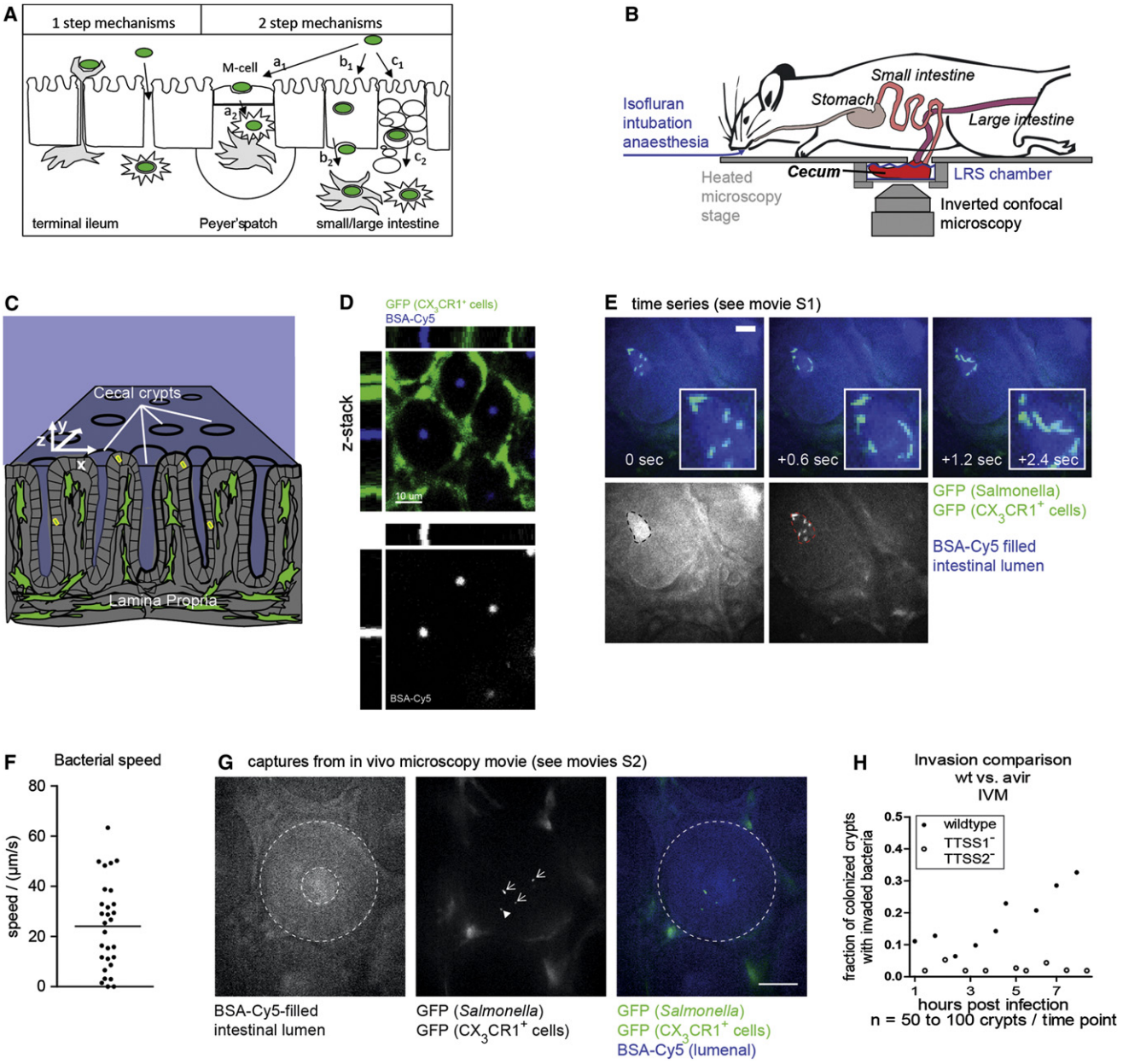

Figure 1. Intravital Microscopy as a Tool to Study the Mechanism of Mucosal *S.* Typhimurium Infection

(A) Plausible *S.* Typhimurium invasion strategies. Transepithelial invasion into the lamina propria can take place in one step (CX3CR1^{high} MΦ extensions; paracellular) or in two steps, i.e., uptake/invasion and a subsequent exit step. It is unclear whether exit might occur via exocytosis (a_2, b_2) or through enterocyte apoptosis (c_2).

(B and C) Intravital microscopy setup (B) and schematic representation of the cecal tissue (C).

(D–F) CX3CR1$^{gfp/+}$ mice infected intragastrically for 5 hr with *S.* Typhimurium (pGFP) were subjected to intravital microscopy. The gut lumen was stained with BSA-Cy5. No leakage of lumenal BSA-Cy5 into the lamina propria was observed (D). Bacterial swimming speed in cecal crypts was determined by time-lapse microscopy (E and F). GFP (*S.* Typhimurium and CX_3CR1^+ cells), green; cecal lumen, blue. Scale bars represent 10 µm (D and E). Horizontal line, median of swimming speeds.

(G and H) Intravital microscopy analysis of invasion of GFP-tagged bacteria injected directly into the cecal lumen. Epithelium invasion depends on *Salmonella* virulence factors (H) but it is independent of CX_3CR1^+ extensions. Arrows, swimming and attaching bacteria in gut lumen; arrowhead, intraepithelial *S.* Typhimurium. GFP (bacteria and CX_3CR1^+ cells), green; BSA-Cy5, blue (cecal lumen). The scale bar represents 20 µm (G).

See also Figure S1 and Movie S1.

within lamina propria phagocytes at later stages (Frost et al., 1997; Hapfelmeier et al., 2005, 2008; Müller et al., 2009; Reis et al., 2003). However, it had remained unclear how *S.* Typhimurium travels to the basolateral side and how the pathogen exits from the enterocyte to reach the lamina propria. It is not known whether pathogen release occurs within apoptotic bodies

formed by the infected enterocyte, by exocytosis at the basolateral side, or by another mechanism (Figure 1A) (Hybiske and Stephens, 2008).

Here, we have employed in vivo microscopy to study the initial steps of cecal mucosa infection by *S.* Typhimurium. This established a virulence function of TTSS-2 in the diarrheal disease, demonstrated how the pathogen exits from the epithelial cell, revealed a sampling pathway in the mucosa, and suggested that *S.* Typhimurium can subvert this pathway in vivo.

RESULTS

Intravital Microscopy Setup for Studying the Cecal *S.* Typhimurium Infection

For our analysis of the infection process, we have adapted the streptomycin mouse model of *S.* Typhimurium diarrhea (Kaiser et al., 2012). In this model, the pathogen colonizes the cecal lumen by 4–6 hr postinfection (p.i.; $>10^7$ cfu/g), invades the mucosa and elicits inflammation by 6–8 hr p.i. (Altmeyer et al., 2010). This was ideal for in vivo microscopy analysis of the initial host-pathogen interaction.

Here, we established an experimental procedure for time-lapse imaging of the bacteria through the wall of the intact cecal tissue (Figure 1B and Figures S1A–S1C available online; Experimental Procedures). This setup allowed us to capture the initial interactions of *S.* Typhimurium with the host's living gut tissue in situ.

Motility of *S.* Typhimurium in the Gut Lumen, Attachment, and Invasion into Enterocytes

First, we employed B6.129P-*CX3CR1*^{tm1Litt}/J mice ($CX_3CR1^{gfp/+}$ [Jung et al., 2000]), which express a bright GFP signal in CX_3CR1^{high} MΦ of the cecal lamina propria (Hapfelmeier et al., 2008). The mice were infected with WT *S.* Typhimurium (Hoiseth and Stocker, 1981) constitutively expressing the green fluorescent protein (pGFP) and the gut lumen was labeled with Cy5-labeled albumin (e.g., Figures 1C and 1D). To monitor bacterial swimming, we used a spinning disc confocal microscope, which allowed imaging at very high frame rates. Later, the data were verified using scanning confocal microscopy. At 4 hr p.i., the bacteria were swimming in the gut lumen and along the epithelial surface at speeds of 5–50 μm/sec (Figures 1E and 1F; Movie S1), which is in the same range as observed for *E. coli* and *S.* Typhimurium swimming in liquid broth media (20–40 μm/s [Magariyama et al., 2001]).

After 4–6 hr p.i., *S.* Typhimurium "stopped" at the epithelial surface and invaded into the epithelium (Figures 1G and 1H; movies not shown). The number of crypts harboring infected enterocytes increased with time, while control infections with an avirulent *S.* Typhimurium mutant (M557; *invGsseD* [Hapfelmeier et al., 2004]), lacking key virulence factors required for tissue invasion, did not (Figure 1H). Thus, we were able to image TTSS-1 driven invasion into epithelial cells of the living gut.

None of these observed invasion events was associated with CX_3CR1^+ MΦ protrusions extending into the epithelial layer or into the gut lumen. This was in line with recent data (Hapfelmeier et al., 2008) and indicated that the observed mechanism of invasion into the cecal mucosa was distinct from the extension-mediated transepithelial transport described for ileal CX_3CR1^{high} cells (Chieppa et al., 2006; Niess et al., 2005).

Further control experiments ruled out that mucosa invasion occurred in a paracellular fashion and confirmed that most (if not all) initial events of mucosa entry by *S.* Typhimurium occurred via invasion into intestinal epithelial cells (Figures S1D–S1G).

Real-Time Analysis of Epithelial Traversal and Entry into the Lamina Propria

Upon invasion into intestinal epithelial cells, we noticed that most bacteria began moving toward the basolateral side. To analyze this process, we have employed double-transgenic p_{vil}*cre* × *dsRed*^{floxSTOP} or p_{vil}*cre* × *tdRFP*^{floxSTOP} mice expressing red fluorescent proteins in intestinal epithelial cells (Experimental Procedures; Figure 2A). The animals were infected with *S.* Typhimurium (p*ssaG*-GFP) and imaged between 5 and 7 hr p.i.

Three categories of intraepithelial bacteria could be discerned (Figures 2B–2E; see also Movie S2): (1) Some of the bacteria remained within the apical half of the epithelial cell (Figures 2B and 2E). (2) A second group of bacteria traversed the epithelium within 2–3 hr. This might resemble earlier data on *Salmonella* transition through epithelial layers in vitro (Finlay et al., 1988). After arrival at the basolateral side, no further movement was observed (Figures 2C and 2E). (3) A third class of bacteria traversed the epithelium, exited at the basolateral side, and entered into the lamina propria (Figures 2D and 2E). Pathogen exit into the lamina propria was verified by in situ staining of lamina propria cells during the course of the intravital microscopy experiment (Figure 2F and Figure S2).

Transepithelial Trafficking Requires TTSS-2

It had remained unclear whether the transepithelial movement of *S.* Typhimurium was affected by bacterial virulence factors. We hypothesized that this might be the case. The type III secretion system-2 was a plausible candidate, as TTSS-2 is known to manipulate vesicular trafficking within infected monocytes (Abrahams et al., 2006; Bakowski et al., 2008; Schroeder et al., 2011). However, it had remained unclear, whether TTSS-2 was affecting the transepithelial trafficking of the pathogen in polarized epithelia.

To analyze the function of TTSS-2, we infected streptomycin-treated p_{vil}*cre* × *tdRFP*^{floxSTOP} mice with WT *S.* Typhimurium (p*ssaG*-GFP) or an isogenic mutant lacking a functional TTSS-2 (M556; *sseD::aphT*; [Hapfelmeier et al., 2004]) and bacterial movement within the cecal epithelium was analyzed at 6–8 hr p.i. by in vivo microscopy (Figure 2G). Strikingly, all M556 bacteria were located at the apical side of the enterocytes, and remained approximately 10–20 μm away from the brush border. In contrast, WT *S.* Typhimurium showed a much broader distribution within the epithelial cells and we observed pathogen movement to the basolateral side ($p = 0.023$ between initial and final distance from brush border; Figure 2H). In line with this, we observed that WT *S.* Typhimurium reached the lamina propria more efficiently than M556 by 8 hr p.i. (data not shown). Thus, TTSS-2 contributes to breaching the gut epithelium.

$CD11c^+CX_3CR1^{high}$ MPs Can Take Up *S.* Typhimurium in the Lamina Propria

Next, we analyzed the lamina propria mononuclear phagocytes (MPs), which take up *S.* Typhimurium after the pathogen has breached the intestinal epithelium. The lamina propria

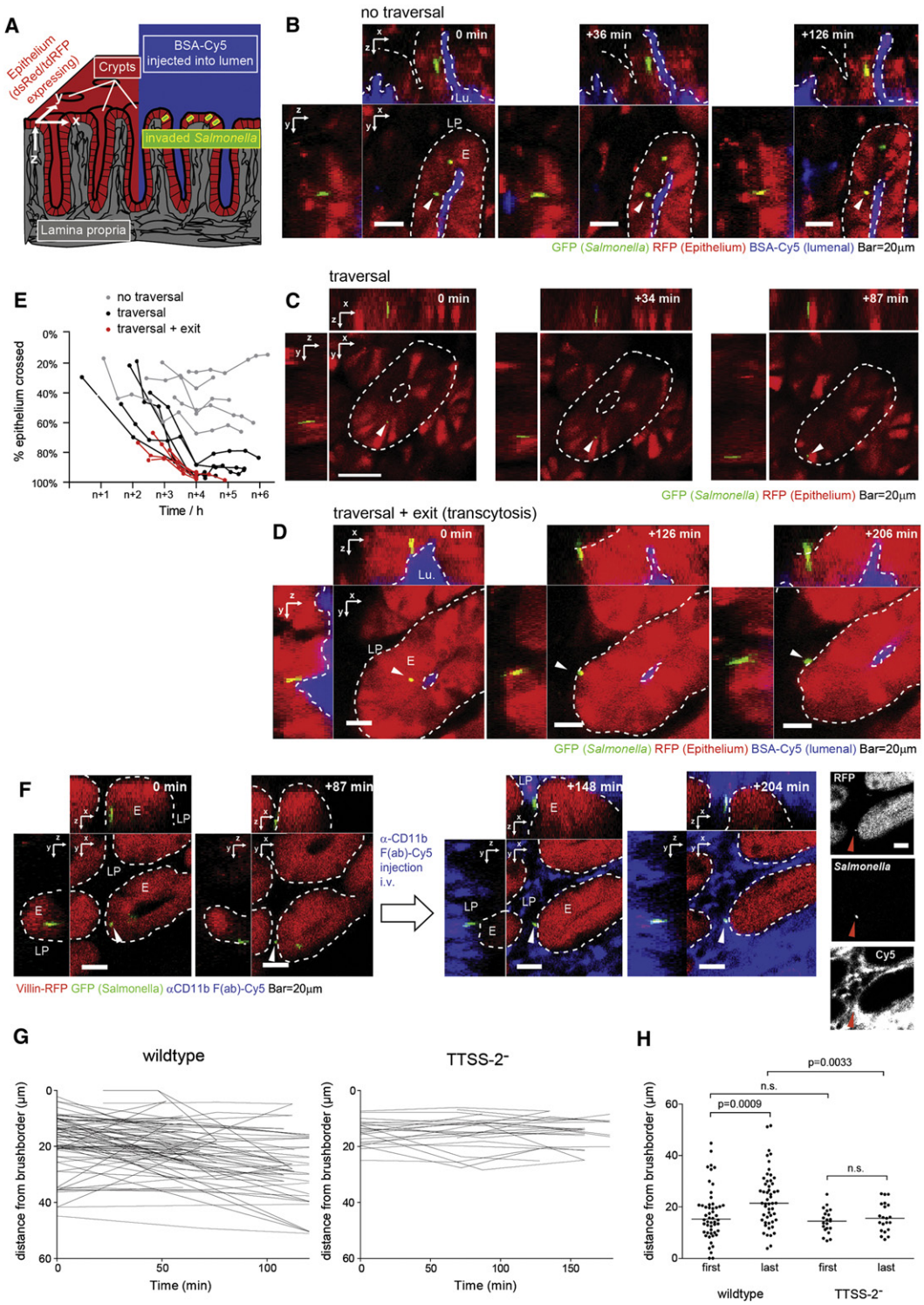

Figure 2. Transcytosis through Cecal Enterocytes Requires TTSS-2

(A) Schematic of the cecal tissue subjected to intravital microscopy.

(B–F) Transgenic mice were infected with *S.* Typhimurium (*pssaG*-GFP) for 4 hr prior to intravital microscopy. BSA-Cy5 was injected into the cecal lumen (B–D) or Cy5-labeled α-CD11b-F(ab') fragments were applied i.v. (F) and served as luminal or lamina propria stain, respectively. Three types of invasion behavior were observed (B–F; arrowheads): (1) no traversal after invasion (B), (2) traversal from apical to basolateral side (C), and (3) transcytosis (epithelial traversal and subsequent exit into the lamina propria) (D and F). RFP (tdRFP or dsRed, intestinal epithelium), red; GFP (*S.* Typhimurium), green; Cy5 (lumen, A and B–D; or lamina propria, F), blue; *tdRFP*- or *dsRed*-expressing epithelium (labeled "E" in images), red. Outlines of the epithelium, the lamina propria (nonfluorescent in B–D, Cy5-labeled in F, "LP") and the intestinal lumen (Cy5-labeled in B–D, "Lu.") are indicated by dashed lines. Scale bars represent 20 μm.

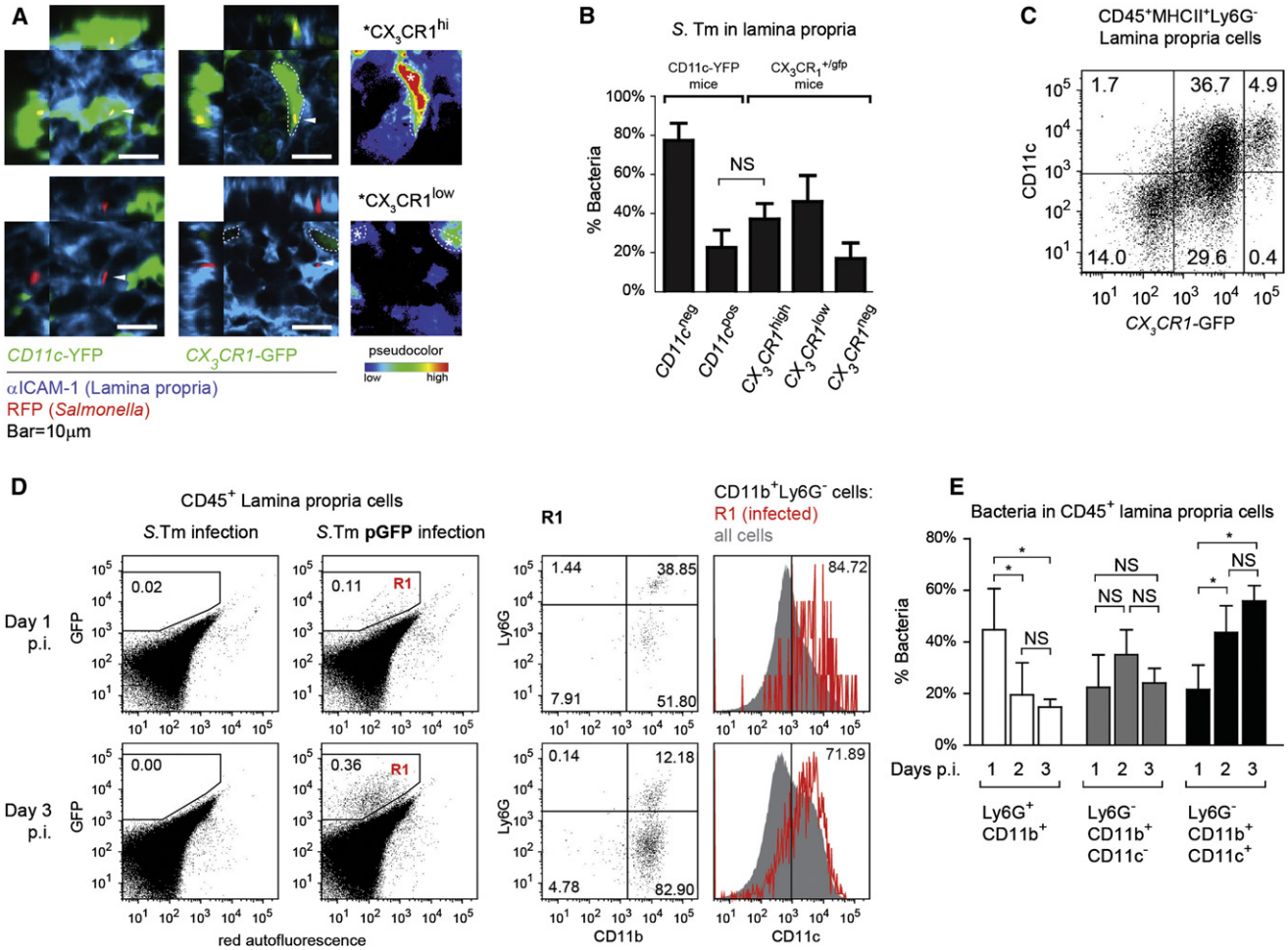

Figure 3. In the Cecal Lamina Propria *S.* Typhimurium Resides within CD11c$^+$CX$_3$CR1^{high} MPs, CX$_3$CR1^{low} tissue MΦ, and Neutrophils

(A and B) CX$_3$CR1$^{gfp/+}$ and CD11c-YFP mice were infected for 24 hr with *S.* Typhimurium (p*ssaG*-mCherry, white arrowheads) and cryosections of cecal tissue were stained with α-ICAM-1 antibodies and analyzed. GFP or YFP (CX3CR1$^+$ or CD11c$^+$ cells, respectively), green; mCherry (*S.* Typhimurium), red; ICAM-1 (lamina propria), blue. Scale bars represent 10 μm. A separate panel shows the GFP channel as a heat map in (A). Averages and standard deviations from at least four individual mice are indicated in (B).

(C) FACS analysis of lamina propria MPs (gated on CD45$^+$MHCII$^+$Ly6G$^-$ cells) revealed a distinct CD11c$^+$CX$_3$CR1^{high} MP population.

(D and E) Distribution of *S.* Typhimurium (p*ssaG*-GFP or untagged, in C57BL/6 mice) at day 1–3 p.i. in CD45$^+$ lamina propria cells as observed by FACS. The *Salmonella*$^+$ gate "R1" was set by comparing mice infected with p*ssaG*-GFP-tagged (D, middle) and untagged (D, left) bacteria. Pathogen distribution between PMNs (Ly6G$^+$CD11b$^+$, open bars), CX$_3$CR1^{low} tissue MΦ (Ly6G$^-$CD11b$^+$CD11c$^-$, shaded bars) and CD11c$^+$ MPs (Ly6G$^-$CD11b$^+$CD11c$^+$, closed bars) is shown in (E). Error bars represent the SD; averages and SD are from at least four individual mice. *p < 0.05; NS, not significant.

CD11c$^+$ MPs in the murine intestine can be functionally subdivided into CD11c$^+$CD103$^+$CX$_3$CR1$^-$ (CD103$^+$ dendritic cells [DCs]) and CD11c$^+$CD103$^-$ CX$_3$CR1^{high} (CX$_3$CR1^{high} MΦ) (Schulz et al., 2009; Varol et al., 2010). In order to investigate whether these MP subsets harbor the pathogen, we infected CX$_3$CR1$^{gfp/+}$ mice and CD11c-YFP mice with *S.* Typhimurium harboring the plasmid p*ssaG*mCherry.

In order to obtain sufficient numbers of events, we chose 1 day infections. Earlier data had indicated that the pathogen resides in the phagocyte initially encountered for at least 24 hr (Hapfelmeier et al., 2008). Thus, the 1 day time point represents a reasonable compromise for identifying the lamina propria phagocytes initially taking up the pathogen. In tissue sections, we detected approximately 35% of the bacteria in CX$_3$CR1^{high} cells, 45% in CX$_3$CR1^{low} cells, and 20% in CX$_3$CR1$^-$ cells (Figures 3A and 3B). Equivalent results were obtained in CD11c-YFP mice (Figure 3B). Furthermore, the fluorescence-activated cell sorting (FACS) analysis of the cecal lamina propria of CX$_3$CR1$^{gfp/+}$ mice

(G) Migration of WT *S.* Typhimurium or M556 toward the basolateral side of the enterocyte. Each line represents one bacterial track.

(H) Statistical analysis of the TTSS-2 dependency. Positional data from (G) (first/last time point of each track) were analyzed with a paired t test (first versus last) or the Mann-Whitney U test (WT versus M556). N.S., not significant.

See also Figure S2 and Movie S2.

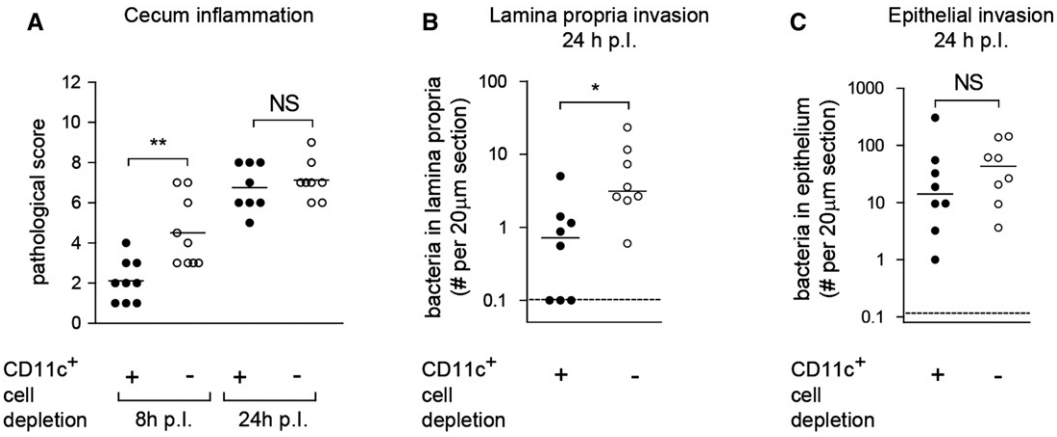

Figure 4. Depletion of CD11c$^+$ MPs Attenuates the Mucosal Infection

CD11c-DTR$^{tg/+}$ (closed circles) and nontransgenic littermate controls (open circles) were injected with DTX and infected with *S.* Typhimurium (p*ssaG*-mCherry) for 8 hr or 24 hr. Gut inflammation (A) was analyzed in HE sections. Bacterial loads in the lamina propria (B) and the epithelium (C) were analyzed by fluorescence microscopy counting mCherry$^+$ bacteria in α-ICAM-1-stained tissue sections (24 hr p.i.). Horizontal lines, median; *p < 0.05; NS, not significant. Each symbol represents one mouse; data are pooled from two independent experiments.

revealed that all CX_3CR1^{high} cells at day 1 p.i. were also CD11c$^+$ (Figure 3C), suggesting that the vast majority of infected CX_3CR1^{high} cells expressed CD11c and hence most likely represented CX_3CR1^{high} MΦ. In contrast, the CD103 marker, though stainable on ileal cells, could not be stained reliably on cecum cells (data not shown). It is unclear whether this was attributable to marker degradation in the inflamed tissue. However, as Varol et al. could clearly show that all CD11c$^+$$CX_3CR1^{high}$ cells in the large intestine are exclusively CD103 negative (Varol et al., 2009), our data indicate that 20%–40% of the bacteria reside within CX_3CR1^{high} MΦ shortly after lamina propria invasion.

FACS analysis of infected cecal lamina propria cells verified the microscopy data. Mice were infected for 1 day with *S.* Typhimurium (p*ssaG*-GFP; n ≥ 4 per group), and cells harboring pathogens were analyzed. Tissues recovered at days 2 and 3 p.i. served as controls and allowed calibrating the FACS detection, as the numbers of infected lamina propria cells were much larger (Figure 3D, bottom panels). Between day 1 and day 3 p.i., all bacteria-containing CD45$^+$ lamina propria cells were CD11b$^+$. At day 1 p.i., *S.* Typhimurium was found in Ly6G$^+$CD11b$^+$CD11c$^-$ polymorphonuclear cells (PMNs), (45% ± 16%), Ly6G$^-$CD11b$^+$CD11c$^-$ tissue MΦ (presumably CX_3CR1^{low}), (22% ± 13%) and in Ly6G$^-$CD11b$^+$CD11c$^+$ cells (most likely CX_3CR1^{high} MΦ, 22% ± 10%), (Figure 3E). These results were in line with the fluorescence microscopy analysis and verified that *S.* Typhimurium resides within granulocytes and MPs soon after entry into the lamina propria. Furthermore, a significant fraction of the infected MPs are CX_3CR1^{high} MΦ.

Depletion of CD11c$^+$ MPs Delays Lamina Propria Colonization and the Onset of Mucosal Inflammation

To address the functional role of lamina propria MPs in the initial phase of mucosal inflammation, we employed a depletion strategy. B6.FVB-Tg(Itgax-DTR/EGFP)^{57Lan}/J (CD11c-DTR^{tg}) mice express a human diphtheria toxin receptor (DTR)-GFP fusion protein in CD11c$^+$ cells. In the cecum tissue, diphtheria toxin (DTX) treatment specifically eliminates all CD11c$^+$ MPs (including CD103$^+$ DCs and CX_3CR1^{high} MΦ) without affecting other lamina propria cell populations (Hapfelmeier et al., 2008).

CD11c-DTR^{tg} mice were injected with DTX and infected with *S.* Typhimurium (p*ssaG*mCherry; n ≥ 8 per group). In the CD11c$^+$ cell-depleted mice, the onset of mucosal inflammation and the colonization of the lamina propria were significantly delayed ($p < 0.05$; Figure 4A,B). In contrast, the epithelial invasion by the pathogen was not affected ($p \geq 0.05$; Figure 4C). This indicated that lamina propria CD11c$^+$ MPs are important for efficient lamina propria colonization by *S.* Typhimurium and for mounting mucosal inflammation within 8 hr of infection. In the depleted mice, MP-independent mechanisms such as the activation of caspase-1 in epithelial cells may step in and initiate a delayed type of tissue inflammation by 24h p.i. (Müller et al., 2009). The nature of these mechanisms remains to be analyzed.

Antibody Coating of Bacteria Reveals that *S.* Typhimurium Reaches the Lamina Propria by Transcytosis

The mechanism of pathogen entry into the lamina propria has remained poorly defined—i.e., it had remained unclear how the pathogen exits from the epithelial cell (see Figure 1A). Epithelial cell death and uptake of pathogen-loaded apoptotic bodies (Huang et al., 2000), release of membrane enclosed pathogens, or release of extracellular bacteria on the basolateral side were conceivable. Only the latter case would result in a transient extracellular state before the bacterium is internalized by lamina propria phagocytes. This was assessed in vivo using an antibody coating strategy: First, we generated an α-*S.* Typhimurium antiserum in IgA$^{-/-}$ knockout mice, which can coat the pathogen's surface as described recently (Experimental Procedures) (Endt et al., 2010). This antiserum, or control serum from naive IgA$^{-/-}$ mice, was transferred into B cell-deficient $J_H^{-/-}$ mice, which are incapable of producing antibodies (C57BL/6 background) (Chen et al., 1993).

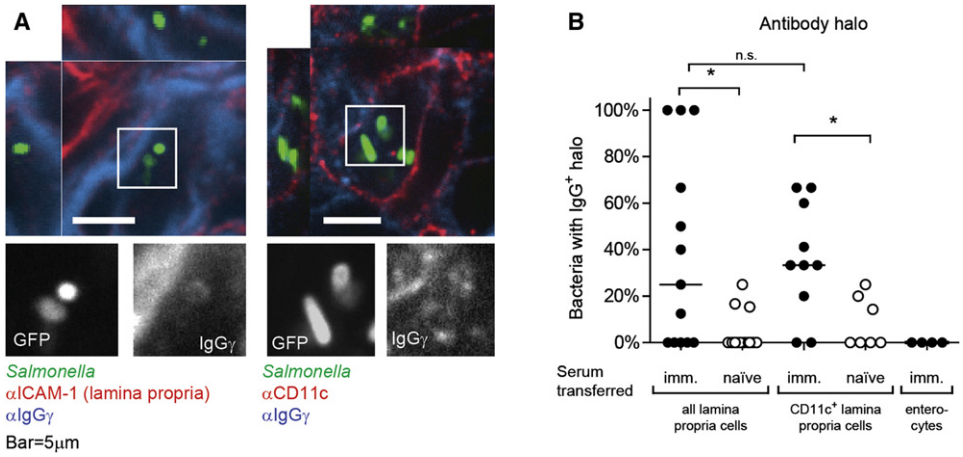

Figure 5. Antibody Coating of Extracellular *S.* Typhimurium in the Lamina Propria

(A) $J_H^{-/-}$ mice were infected with *S.* Typhimurium (p*ssaG*-GFP) and injected with α-*S.* Typhimurium antiserum (closed circles; from $IgA^{-/-}$ mice) or naive controls 12 hr later. Animals were sacrificed 24 hr p.i., and 20 μm cecal cryosections were stained (α-ICAM-1-Cy3 or α-CD11c-Cy3 and α-IgG2cγ-Cy5). Scale bars represent 5 μm.

(B) The presence of α-IgG2cγ-Cy5 halos around GFP^+ bacteria in LP (at least seven stacks/group). Each symbol represents one confocal stack. Negative controls, injection of naive serum or imaging of bacteria located in ICAM-1 negative enterocytes. Horizontal lines, median; *, $p < 0.05$; NS, not significant.

The mice were infected for 24 hr with *S.* Typhimurium (p*ssaG*-GFP). In the mice injected with the α-*S.* Typhimurium LPS antiserum (but not the controls; open symbols), α-IgG2cγ staining revealed antibody halos surrounding the bacteria residing within lamina propria cells ($p < 0.05$; Figure 5A). No halos were detected around bacteria localized within epithelial cells, indicating that antibody coating occurs at the release into the lamina propria (Figure 5B). This suggested that, after entering the lamina propria, the bacteria undergo an extracellular state before entering into lamina propria cells.

In summary, these data implied that *S.* Typhimurium can reach the lamina propria by transcytosis, i.e., invasion at the apical side of epithelial cells, migration to the basolateral side, and exocytosis into the interstitial space of the lamina propria.

Lamina Propria MPs Sample *S.* Typhimurium and Epithelial Cell Material

During intravital microscopy of *S.* Typhimurium-infected p_{vil}*cre* × *dsRed*^{floxSTOP} or p_{vil}*cre* × *tdRFP*^{floxSTOP} mice, we observed infected and noninfected epithelial cells releasing RFP^+ material at the basolateral side into the lamina propria (Figure 6A). These $dsRed^+$ or $tdRFP^+$ "epithelial bodies" grew over minutes to hours, reached sizes of up to several micrometers in diameter, and detached from the overlying epithelium. Immunofluorescence microscopy using an epithelium-specific α-EpCAM (CD326) antibody verified their epithelial origin (Figure 6B). It seemed plausible that such epithelial bodies might serve the presentation of enterocyte material to the gut immune system, as earlier work had described such a mechanism in the rat intestine (Huang et al., 2000). Due to the potential importance of such a mechanism, we decided to follow up on this initial observation and investigated potential links to the mucosal *S.* Typhimurium infection.

First, we performed high-resolution fluorescence microscopy of fixed tissue sections from *S.* Typhimurium (p*ssaG*-GFP)-infected p_{vil}*cre* × *dsRed*^{floxSTOP} mice (Figure 6C; 12 hr p.i.). Staining of the lamina propria cell surface marker ICAM-1 allowed colocalization analysis of *S.* Typhimurium (p*ssaG*-GFP; green) and RFP^+ epithelial bodies within cells of the lamina propria. Strikingly, numerous *Salmonella*-containing lamina propria cells harbored at the same time RFP^+ epithelial bodies (Figures 6C–6E). To control for background fluorescence, we took advantage of the mosaic-like expression pattern of the *dsRed* in p_{vil}*cre* × *dsRed*^{floxSTOP} mice. No RFP^+ epithelial bodies were detected in infected (and noninfected) lamina propria cells underneath RFP^- areas of the epithelium (Figure 6D). Furthermore, quantitative colocalization analysis of green (*S.* Typhimurium p*ssaG*-GFP) and red (epithelial-derived dsRed) fluorescence verified that approximately half of the bacteria in the lamina propria were clearly colocalized with epithelial cell material ($p < 0.05$; Figure 6E). Whether background fluorescence might have prevented detection of weak red fluorescence signals from small, RFP^+ epithelial bodies in the other half of the bacteria infected cells remains unclear. In any case, the large proportion of bacteria in the lamina propria localized within cells sampling epithelial cell material suggests that *S.* Typhimurium may lodge onto an epithelium-sampling mechanism of the intestinal immune system.

Epithelial Material Release Is a Constitutive Process

It had remained unclear whether the *S.* Typhimurium infection may enhance the release of epithelial material into the lamina propria, thus amplifying a homeostatic sampling pathway (Huang et al., 2000; Niess et al., 2005). Based on the apoptotic nature of the epithelial cell material previously reported by Huang et al. (2000) and the ability of *S.* Typhimurium to activate cell death pathways in epithelial cells (Müller et al., 2009), we speculated that release of epithelial bodies and the concomitant release of the pathogen might be attributable to pathogen-induced enterocyte cell death. However, the pan-caspase inhibitor Z-VAD-fmk affected neither the frequency of phagocytes harboring both epithelial bodies and *S.* Typhimurium nor the

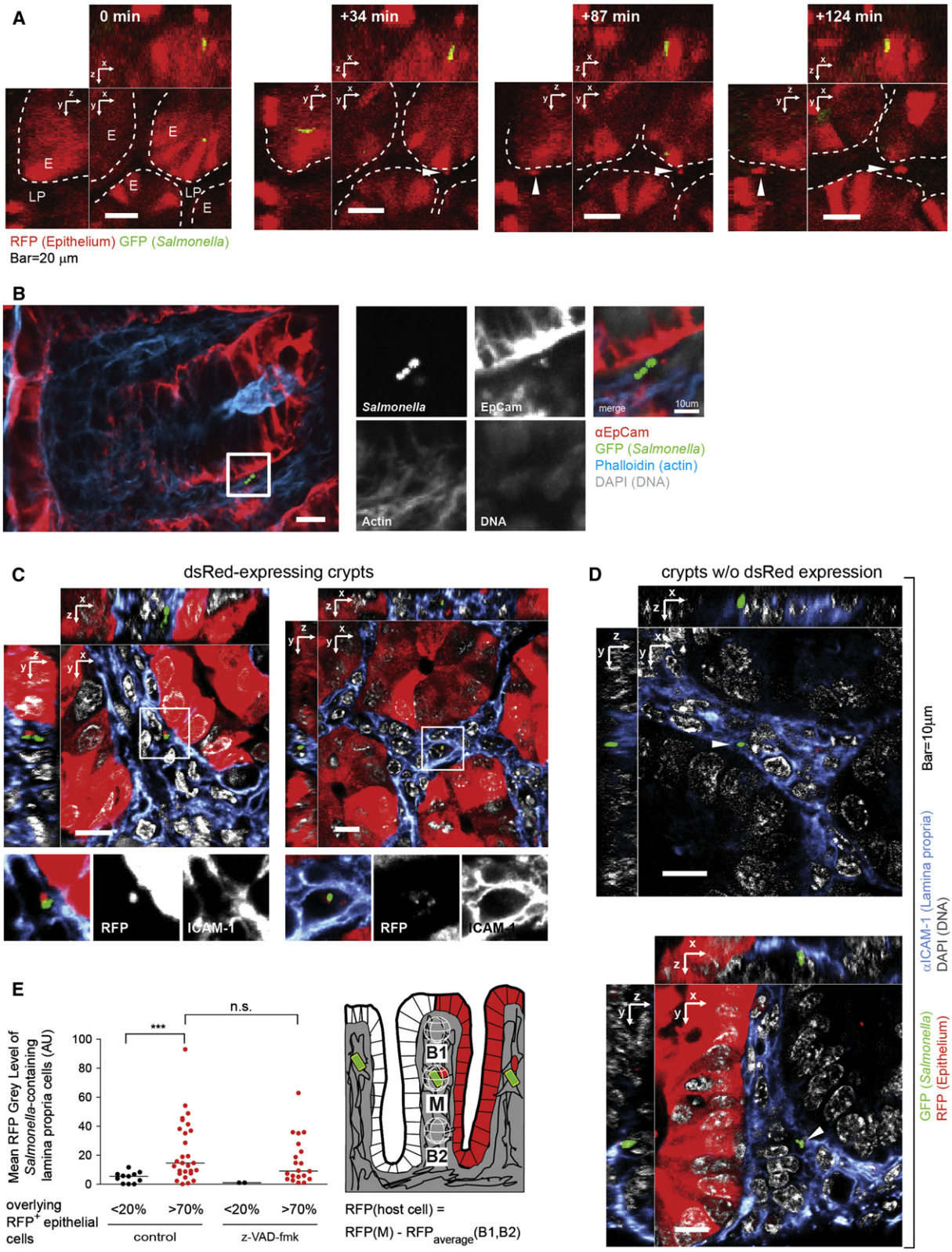

Figure 6. Epithelial Material Is Released at the Basolateral Side of Enterocytes

$p_{vil}cre \times dsRed^{loxSTOP}$ mice were infected with *S.* Typhimurium (*pssaG*-GFP).

(A) Intravital microscopy (from 4 hr p.i. on) of a growing RFP^+ body (white arrowhead) in the lamina propria. Epithelium ("E") and lamina propria ("LP") are outlined. Scale bars represent 20 μm.

rate of gut tissue invasion (Figure 6E and Figure S3). Nevertheless, the number of TUNEL-positive epithelial cells was significantly reduced in these animals (Figure S3). Thus, the epithelial material observed in the *Salmonella*-containing lamina propria cells was not attributable to enterocyte cell death. It is likely of different origin than the epithelial material reported earlier in rat intestinal phagocytes (Huang et al., 2000).

In a second approach, we asked whether pathogen-inflicted pathology would affect the rate of epithelial body release. For this purpose, we have quantified the epithelial body content of lamina propria cells by microscopy. p_{vil}*cre* × *dsRed*^{floxSTOP} mice were infected with WT *S.* Typhimurium or an avirulent mutant [S.Tm^{avir} (SB161, *invG*) (Kaniga et al., 1994)], and we quantified the amount of RFP$^+$ bodies in lamina propria cells beneath RFP-expressing epithelial crypts (Figures 7A and 7B, red histograms). RFP$^-$ crypts served as an internal control (Figure 7B, gray histograms). RFP$^+$ epithelial bodies were specifically detected in lamina propria cells beneath RFP$^+$ crypts in both groups of mice ($p < 0.05$; Figure 7B, red versus gray). Equivalent data were obtained in FACS analyses (Figure S4). In all our FACS experiments, approximately 1%–4% of all CD45.1$^+$ lamina propria cells were found to harbor detectable amounts of RFP$^+$ epithelial cell material (Figures 7C and 7D and Figure S4). Finally, the release of RFP$^+$ bodies from noninfected crypts was also verified by in vivo microscopy (data not shown). Therefore, epithelial material release from the basolateral side of the cecal epithelium is a frequent event and occurs in the inflamed and in the noninflamed mucosa, alike.

Distribution of Epithelial Bodies and of Bacteria within Lamina Propria Phagocytes

FACS analysis was performed in order to identify the lamina propria cell populations harboring the epithelial bodies. First, we analyzed cecum lamina propria phagocytes isolated from noninfected p_{vil}*cre* × *dsRed*^{floxSTOP} mice. A significant fraction of CD45$^+$ cells harbored RFP$^+$ material (~1%; Figure 7C). Of these CD45$^+$RFP$^+$ cells, approximately half were CD11b$^+$CD11c$^-$ (presumably CX_3CR1^{low} tissue MΦ), half were CD11b$^+$CD11c$^+$ cells (CX_3CR1^{high} MΦ and DCs; ~20% each; Figure 7C), while PMN (Ly6G$^+$ cells) were absent from the noninfected mucosa. These data verified the uptake of epithelial bodies by lamina propria tissue MΦ, CX_3CR1^{high} MΦ, and DCs under steady-state conditions.

Next, we analyzed the distribution of epithelial material in phagocytes of the inflamed mucosa infected by WT *S.* Typhimurium. In order to ensure that all red fluorescent signals were derived from uptake (and not from erroneous cell-intrinsic expression), we lethally irradiated p_{vil}*cre* × *tdRFP*^{floxSTOP} mice (CD45.2$^+$, C57BL/6 background) or control C57BL/6 mice and reconstituted them with bone marrow from congenic WT CD45.1$^+$ animals and focused our analysis on the CD45.1$^+$ cells. These chimaeric mice were infected for 24 hr with WT *S.* Typhimurium (p*ssaG*-GFP). As expected, the infected lamina propria yielded much higher numbers of CD45$^+$ cells including high numbers of Ly6G$^+$ PMNs, which are absent from the noninflamed lamina propria.

Among the CD45.1$^+$ (CD45$^+$ CD45.2$^-$) cells harboring RFP$^+$ material (Figure 7D), approximately 80% were found to be CD11b$^+$Ly6G$^+$ cells (PMNs), 10% Ly6G$^-$CD11b$^+$CD11c$^-$ cells (tissue MΦ) and 10% Ly6G$^-$CD11b$^+$CD11c$^+$ cells (CX_3CR1^{high} MΦ and DCs). Reanalysis of the same FACS data with respect to pathogen-containing cells (GFP$^+$; Figure 7E, bottom panels) revealed that *S.* Typhimurium (p*ssaG*-GFP) had a strikingly similar cellular distribution as the epithelial bodies (Figures 7D and 7F), i.e., being detected mainly in PMNs and to a lesser extent in both MΦ and DCs. However, the fraction of PMN-localized bacteria was slightly lower, while the fraction of MΦ- and DC-localized bacteria was slightly higher than in the case of the epithelial bodies. These data suggested that both extracellular bacteria and epithelial bodies are taken up randomly by lamina propria phagocytes. However, their respective half-lives/persistence/growth rates might differ slightly within the different phagocyte cell types. In any case, the uptake of epithelial material by lamina propria MPs represents a physiological, constitutive process, which is hijacked by *S.* Typhimurium in order to colonize the lamina propria.

DISCUSSION

We found that *S.* Typhimurium infects the cecal mucosa via a two-step mechanism and identified three mechanistic features of this process: (1) TTSS-2 dependent traversal to the basal side, (2) exocytotic release into the lamina propria, and (3) uptake by lamina propria phagocytes (including CX_3CR1^{high} MΦ) together with epithelial bodies shed from the basolateral side of the epithelium, suggesting that the pathogen lodges onto an epithelium-sampling pathway for colonization of the lamina propria.

Intriguingly, the invasion mechanisms seem to differ between different sites of the intestinal tract (Figure 1A). This might be attributable at least in part to the competitive effects of the microbiota and to functional differences of mucosal MP subsets organizing defense at each particular site. In the classical typhoid fever model, pathogen growth in the large intestine is inhibited by the resident microflora ("colonization resistance" [Stecher and Hardt, 2011]) and invasion occurs mainly in the small intestine (Jones et al., 1994; Kohbata et al., 1986; Santos et al., 2002; Tsolis et al., 1999). Direct, transepithelial sampling of CX3CR1^{high} cells was observed in the terminal ileum and may occur as early as 30 min p.i (Chieppa et al., 2006; Niess et al., 2005; Vazquez-Torres et al., 1999; Worley et al., 2000).

(B) Colocalization of EpCam-positive material (red) with *S.* Typhimurium (green) in LP (α-ICAM-1, blue; DAPI, gray). Scale bars represent 10 μm.
(C–E) Analysis of RFP$^+$ material in the vicinity of *S.* Typhimurium in the lamina propria (α-ICAM-1-Cy5, DAPI). (C) shows LP-resident *S.* Typhimurium below areas of *dsRed* expressing epithelium. (D) presents the same animal as (C), showing epithelial areas w/o *dsRed* expression. Epithelium (dsRed, tdRFP), red; *S.* Typhimurium (GFP), green; LP (ICAM-1), blue; DAPI (nuclei), white. Scale bars represent 10 μm.
(E) Colocalization analysis of *S.* Typhimurium and RFP$^+$ epithelial bodies. Controls with z-VAD-fmk treated mice yielded equivalent results. Black, cells underlying epithelial regions without *dsRed* expression (<20% *dsRed*-expressing cells); red, bacteria below regions with *dsRed* expression (>70% *dsRed*-expressing enterocytes). Horizontal lines, median; *$p < 0.001$. Data originates from at least four animals/group.
See also Figure S3.

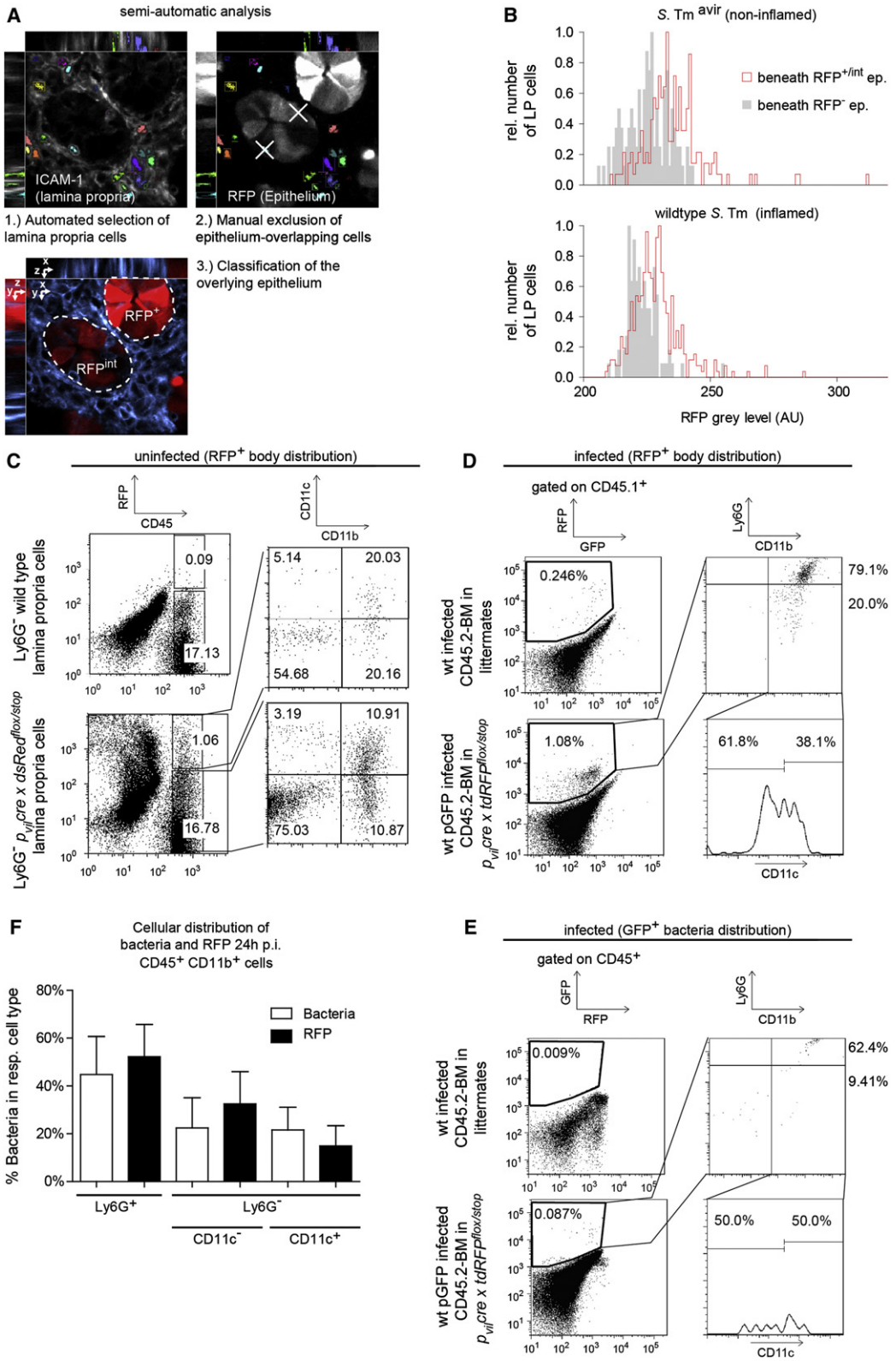

Figure 7. Sampling of Enterocyte Material Is a Constitutive Process and Occurs within Cell Types Also Taking Up Bacteria

(A and B) Quantification of enterocyte material release into the lamina propria. In 3D stacks of fixed tissue, 5–20 cells per stack were automatically drawn, verified manually (i.e., nonoverlapping with epithelium), and classified into cells beneath RFP$^{+/int}$ or RFP^{-} epithelium. RFP-normalized gray level distributions of lamina propria cells beneath RFP$^{+/int}$ epithelium and RFP^{-} epithelium are shown.

Finally, transepithelial invasion has been observed in various animal models for diarrheal disease (Fromm et al., 1974; Frost et al., 1997; Giannasca and Neutra, 1993; Reed et al., 1986; Takeuchi, 1967; Turnbull and Richmond, 1978; Wallis et al., 1986; Watson et al., 1995) including the streptomycin mouse model (Figure 1A) (Kaiser et al., 2012).

Earlier work had shown TTSS-1 mediated enterocyte invasion, pathogen movement to the basal side and the appearance of *Salmonella* spp. in lamina propria phagocytes a few hours post infection (Frost et al., 1997; Hapfelmeier et al., 2004, 2005; Müller et al., 2009; Reis et al., 2003; Takeuchi, 1967; Watson et al., 2005). However, the virulence factors driving transcellular traffic in vivo and the nature of the release step into the lamina propria had remained unclear.

We found that the transepithelial traffic requires TTSS-2. So far, TTSS-2 had been implicated in the manipulation of microtubule-directed traffic within phagocytes, facilitating the formation of *Salmonella*-induced filaments, avoidance of killing by reactive oxygen or nitrogen species of phagocytes, and pathogen traffic toward a perinuclear location, thus enhancing intraphagocyte growth at systemic sites and in the lamina propria (Garcia-del Portillo et al., 1993; Hapfelmeier et al., 2005, 2008; Hensel et al., 1995; Ramsden et al., 2007; Schroeder et al., 2011). Here, we show that TTSS-2 contributes to the diarrheal disease not just by fostering growth in lamina propria phagocytes (Hapfelmeier et al., 2008; Hapfelmeier et al., 2005), but also by enhancing the transepithelial passage, presumably along the enterocyte's microtubular network.

The enterocyte microtubule network is quite different from the radial, centrosome-organized microtubule network in phagocytes and fibroblasts and includes microtubule networks of mixed polarity underneath the apical- and basolateral enterocyte surfaces and polarized microtubules spanning from the apical to the basolateral side (Bré et al., 1987; Meads and Schroer, 1995; Reilein et al., 2005). It will be an interesting task for future work to identify how TTSS-2 effectors manipulate intracellular traffic within this peculiar type of microtubule network.

After completion of epithelial transcytosis and the release into the interstitial space, the extracellular pathogens are internalized by lamina propria phagocytes, including mucosal CX_3CR1^{high} MΦ. This tissue invasion pathway is clearly different from MP-mediated transport via transepithelial extensions described for the ileal part of the small intestine (Chieppa et al., 2006; Niess et al., 2005; Vallon-Eberhard et al., 2006), or paracellular penetration of the epithelial layer (Finlay et al., 1988; Jepson et al., 1995; Tafazoli et al., 2003).

In the cecal lamina propria, the pathogen distribution between PMNs, tissue macrophages, and CX_3CR1^{high} MΦ was roughly reflecting the relative abundance of these cell types. This suggests that pathogen uptake is a nonselective process initiated by any pathogen-phagocyte encounter. Cecal CX_3CR1^{high} MΦ harbored 20% of the pathogens at 8–24 hr p.i. and represented the major fraction of infected $CD11c^+$ cells at this time point. The finding that $CD11c^+$ cell depletion reduced lamina propria pathogen loads by 5-fold (Figure 4) thus indicates that CX_3CR1^{high} MΦ might represent a "safe haven" for the pathogen. This would be in line with data on Peyer's patch monocytes (Cheminay et al., 2004; Cheminay et al., 2005). At the same time, $CD11c^+$ cell depletion blunted the early onset of overt tissue inflammation. Thus, mucosal $CD11c^+$ cells seem to play a key role in mounting immune defense in response to acute infection. Future work will have to define their precise role in this process (see the Supplemental Discussion for a detailed discussion).

To our surprise, we observed that approximately 1%–4% of all lamina propria phagocytes harbored epithelial cell material released from the basolateral side of the absorptive epithelium. The release of these epithelial bodies was independent of caspase cell death and occurred in a constitutive fashion. Thus, it is clearly distinct from the apoptotic enterocyte material detected earlier in rat lamina propria phagocytes (Huang et al., 2000). The distribution of the epithelial bodies in the different lamina propria phagocyte population was equivalent to the relative abundance of the respective cell types. Therefore, the uptake of the epithelial bodies seems to represent a random process initiated by the next phagocyte nearby. It is tempting to speculate that this process, i.e., the uptake of epithelial cell material into CX_3CR1^{high} MΦ, represents an epithelium-sampling pathway, allowing the mucosal immune system to detect epithelial infection or other stress and respond accordingly. As *S.* Typhimurium was frequently found to colocalize with epithelial material within one and the same lamina propria phagocyte (Figures 5B, 6, and 7), we propose that the pathogen might lodge on the second step of this pathway (i.e., uptake of particulate material by lamina propria CX_3CR1^{high} MΦ) as part of its infection process.

In summary, our work provides important mechanistic information on *S.* Typhimurium invasion into the absorptive epithelium. Clearly, the same pathogen relies on different MP functions for invading different sites of the intestinal mucosa. In the cecal mucosa, *S.* Typhimurium employs active, pathogen-driven transcytosis to access the lamina propria, where it is taken up along with shed epithelial cell material by phagocytic cells, including CX_3CR1^{high} MΦ, which are critical for efficient colonization of the mucosa. The pathogen may subvert a constitutive immune surveillance system for infecting the cecal mucosa. It will be of great interest to decipher this surveillance mechanism, to find out whether similar mechanisms might operate at different anatomical sites and to understand its importance for controlling microbial spread or maintaining mucosal homeostasis.

EXPERIMENTAL PROCEDURES

Bacterial Strains

WT *S.* Typhimurium SL1344 and isogenic strains SB161 (Δ*invG*), M556 (*sseD*), and M557 (Δ*invGsseD*) have been described previously (Hapfelmeier et al.,

(C) FACS analysis of uninfected $p_{vil}cre \times dsRed^{floxSTOP}$ mice (lower-left panel) shows accumulation of RFP^+ bodies in $CD45^+CD11b^+$ cells.
(D and E) Lethally irradiated $p_{vil}cre \times tdRFP^{floxSTOP}$ mice reconstituted with CD45.1 bone marrow were infected with WT *S.* Typhimurium (p*ssaG*-GFP). Lamina propria cells were stained for CD45, CD45.2, Ly6G, CD11c, and CD11b. CD45.1-reconstituted nontransgenic littermates (D, left, first panel from top) or mice infected with untagged bacteria (D, left, third panel from top) served to set the gates for RFP^+ or GFP^+ cells, respectively. Independent experiments yielded equivalent results. Error bars represent the SD.
See also Figure S4.

2004; Hoiseth and Stocker, 1981; Kaniga et al., 1994). The GFP plasmids pM973, pM975, pM979, pM1321, and pM2121 have been described previously or constructed herein (see the Supplemental Experimental Procedures for details) (Hapfelmeier et al., 2004; Hapfelmeier et al., 2005; Schlumberger et al., 2007; Stecher et al., 2004). Bacteria were grown in LB (0.3 M NaCl), subcultured for 4 hr, and suspended in cold PBS as described (Hapfelmeier et al., 2004).

Mice and Infection Experiments

All mice were SPF. Experiments were approved (licenses 201/2004, 201/2007, 223/2010, Kantonales Veterinäramt Zürich) and performed as legally required.

Mouse lines are described in detail in the Supplemental Experimental Procedures. In brief, the following lines were used: C57BL/6 (WT), Igh-J^{tm1Dhu} ($J_H^{-/-}$), Igh-2^{tm1Grh} (IgA$^{-/-}$), B6.SJL-Tg(Vil-cre)^{997Gum}/J (p_{vil}*cre*), B6;129S6-Tg(ACTB-Bgeo,-DsRed*MST)^{1Nagy}/J (*dsRed*^{floxSTOP}), B6-Tg(ROSA-tdRFP) (tdRFP^{floxSTOP}), B6.129P-*CX3CR1*^{tm1Litt}/J ($CX_3CR1^{gfp/gfp}$), B6.FVB-Tg(Itgax-DTR/EGFP)^{57Lan}/J (CD11c-DTR^{tg}), and B6-Tg(Itgax-EYFP).

Streptomycin-pretreated mice (20 mg/animal) were infected by gavage (5×10^7 cfu) (Barthel et al., 2003; Hapfelmeier et al., 2008). Live bacterial loads (cfu) were determined by plating (Hapfelmeier et al., 2008), and HE-stained tissues were scored as described, by evaluation of submucosal edema, PMN infiltration, goblet cells, and epithelial damage (Barthel et al., 2003).

In Vivo Microscopy

The procedure is described in detail in the Supplemental Experimental Procedures. In brief, the animals were anaesthetized, intubated, respired with oxygen (1.8%–2.0% Isofluran), and mounted on a temperature-controlled microscopy stage, and the cecum was surgically exposed and placed in a glass-bottom chamber filled with Ringer/lactate solution. Where indicated, 100 μl PBS (5 μg/ml TRITC-albumin; Sigma-Aldrich) was injected into the cecum lumen. Peristalsis was controlled via Buprenorphin (0.3 mg/kg, s.c.; Temgesic, Essex Chemie, Luzern, Switzerland).

Imaging was performed with a Zeiss Axiovert 200 microscope, an Ultraview confocal head (PerkinElmer), and a krypton argon laser (643-RYB-A01, Melles Griot, Didam, The Netherlands) or a Zeiss LSM510 NLO Meta system with an argon laser (488 nm; green), a HeNe laser (543 nm, 633 nm; red, infrared) and a Cameleon MP two photon laser (720 nm). Image sequences were aligned using the StackReg and TurboReg plugins (Thevenaz et al., 1998) of the ImageJ software (National Institutes of Health, http://rsb.info.nih.gov/ij/). Images were processed and evaluated with Volocity 5.0.3. (Improvision, Coventry, UK).

Conventional Immunofluorescence Microscopy

Immunofluorescence microscopy experiments were performed as described (Hapfelmeier et al., 2008). For details, see the Supplemental Experimental Procedures. In brief, parafolmaldehyde-fixed cryosections were blocked (10% goat serum, PBS) and stained with armenian hamster-α-ICAM-1 (Clone 3E2, Becton Dickinson), armenian hamster α-CD11c (Clone HL3, Becton Dickinson), biotin-conjugated α-CD326 (EpCAM, clone G8.8, BioLegend), or biotin-conjugated α-mouse IgG2cγ F(ab')$_2$ fragments (Jackson ImmunoResearch), Cy3- or Cy5-conjugated goat-α-armenian hamster Ig (Jackson Immunoresearch), Streptavidin-647 or Streptavidin-547 (Fluoprobes), Phalloidin-647 (Fluoprobes), and DAPI (Sigma-Aldrich) and imaged with the Zeiss Axiovert 200 Ultraview confocal system. Images were transformed to the colors indicated, superimposed, 3D-reconstructed (where applicable), and deconvoluted with Volocity 5.0.3. (Improvision, Coventry, UK).

Bacteria in the epithelium and lamina propria were enumerated as described (Hapfelmeier et al., 2008). Ten nonserial sections per cecum (or ≥100 bacteria) were analyzed.

Antibody Coating

Twelve hour after infection of $J_H^{-/-}$ mice with *S.* Typhimurium (p*ssaG*-GFP), 250 μl α-S. Typhimurium antiserum serum (from IgA$^{-/-}$ mice; see the Supplemental Experimental Procedures) was administered i.v. At 24 hr p.i., the cecal tissue was fixed, permeabilized, and stained with α-IgG2cγ-Cy5. Halos were enumerated in a blinded manner from at least seven high-magnification (400×) confocal stacks per group recorded around GFP-expressing bacteria in the lamina propria.

FACS

FACS was performed as described in the Supplemental Experimental Procedures. In brief, cecal lamina propria leukocytes were prepared from chopped tissue with Liberase (50 μg/ml) and DNase I (20 μg/ml), passed through an 18 gauge syringe and a 100 μm nylon Cell Strainer, and purified on a Percoll gradient (30% on 100%, iso-osmolar in PBS). The 30%/100% Percoll interphase was harvested and washed, and F_c receptors were blocked (F_c Block, BD Biosciences). The following antibodies were used for staining: PE- and Pe-Cy7-labeled α-Ly6G (clone 1A8), Pe-Cy7- and Pacific blue-labeled α-CD11c (clone HL3; BD PharMingen), PerCP- and Pacific Blue-labeled α-CD45 (clone 30-F11), and PerCP- and APC-Cy7-labeled α-CD11b (clone M1/70; BioLegend). Cells were analyzed on a LSR2 7-color flow cytometer (Becton Dickinson) and processed with the Flowjo software (Treestar).

Statistical Analysis

Statistical analysis was performed with the exact Mann-Whitney U test or paired t test (Prism Version 5.0) for paired data points. $p < 0.05$ (two-tailed) was considered as statistically significant as described (Barthel et al., 2003).

SUPPLEMENTAL INFORMATION

Supplemental Information includes Supplemental Discussion, Supplemental Experimental Procedures, four figures, and two movies and can be found with this article online at doi:10.1016/j.chom.2011.11.013.

ACKNOWLEDGMENTS

We are grateful to S. Hapfelmeier, S. Jung, M. Rescigno, E. Slack, and Hardt lab members for critical discussions. Technical support from G. Csucs and J. Kusch (Light Microscopy Center) and the staff of the RCHCI team, i.e., J. Fehr and S. Freedrich, is gratefully acknowledged. This work was supported by grants to W.D.H. from the Swiss National Science Foundation (310000-113623/1, 310030-132997/1), the Novartis Foundation (number 10A15), and the ETH Zürich research foundation (TH-14/05-2).

Received: February 10, 2011
Revised: October 3, 2011
Accepted: November 7, 2011
Published: January 18, 2012

REFERENCES

Abrahams, G.L., Müller, P., and Hensel, M. (2006). Functional dissection of SseF, a type III effector protein involved in positioning the salmonella-containing vacuole. Traffic *7*, 950–965.

Altmeyer, M., Barthel, M., Eberhard, M., Rehrauer, H., Hardt, W.D., and Hottiger, M.O. (2010). Absence of poly(ADP-ribose) polymerase 1 delays the onset of Salmonella enterica serovar Typhimurium-induced gut inflammation. Infect. Immun. *78*, 3420–3431.

Bakowski, M.A., Braun, V., and Brumell, J.H. (2008). Salmonella-containing vacuoles: directing traffic and nesting to grow. Traffic *9*, 2022–2031.

Barthel, M., Hapfelmeier, S., Quintanilla-Martínez, L., Kremer, M., Rohde, M., Hogardt, M., Pfeffer, K., Rüssmann, H., and Hardt, W.D. (2003). Pretreatment of mice with streptomycin provides a Salmonella enterica serovar Typhimurium colitis model that allows analysis of both pathogen and host. Infect. Immun. *71*, 2839–2858.

Bré, M.H., Kreis, T.E., and Karsenti, E. (1987). Control of microtubule nucleation and stability in Madin-Darby canine kidney cells: the occurrence of noncentrosomal, stable detyrosinated microtubules. J. Cell Biol. *105*, 1283–1296.

Cheminay, C., Chakravortty, D., and Hensel, M. (2004). Role of neutrophils in murine salmonellosis. Infect. Immun. *72*, 468–477.

Cheminay, C., Möhlenbrink, A., and Hensel, M. (2005). Intracellular Salmonella inhibit antigen presentation by dendritic cells. J. Immunol. *174*, 2892–2899.

Chen, J., Trounstine, M., Alt, F.W., Young, F., Kurahara, C., Loring, J.F., and Huszar, D. (1993). Immunoglobulin gene rearrangement in B cell deficient mice generated by targeted deletion of the JH locus. Int. Immunol. *5*, 647–656.

Chieppa, M., Rescigno, M., Huang, A.Y., and Germain, R.N. (2006). Dynamic imaging of dendritic cell extension into the small bowel lumen in response to epithelial cell TLR engagement. J. Exp. Med. *203*, 2841–2852.

Coburn, B., Li, Y., Owen, D., Vallance, B.A., and Finlay, B.B. (2005). Salmonella enterica serovar Typhimurium pathogenicity island 2 is necessary for complete virulence in a mouse model of infectious enterocolitis. Infect. Immun. *73*, 3219–3227.

Endt, K., Stecher, B., Chaffron, S., Slack, E., Tchitchek, N., Benecke, A., Van Maele, L., Sirard, J.C., Mueller, A.J., Heikenwalder, M., et al. (2010). The microbiota mediates pathogen clearance from the gut lumen after non-typhoidal Salmonella diarrhea. PLoS Pathog. *6*, e1001097.

Finlay, B.B., Gumbiner, B., and Falkow, S. (1988). Penetration of Salmonella through a polarized Madin-Darby canine kidney epithelial cell monolayer. J. Cell Biol. *107*, 221–230.

Fromm, D., Gianella, R.A., Formal, S.B., Quijano, R., and Collins, H. (1974). Ion transport across isolated ileal mucosa invaded by salmonella. Gastroenterology *66*, 215–225.

Frost, A.J., Bland, A.P., and Wallis, T.S. (1997). The early dynamic response of the calf ileal epithelium to Salmonella typhimurium. Vet. Pathol. *34*, 369–386.

Garcia-del Portillo, F., Zwick, M.B., Leung, K.Y., and Finlay, B.B. (1993). Salmonella induces the formation of filamentous structures containing lysosomal membrane glycoproteins in epithelial cells. Proc. Natl. Acad. Sci. USA *90*, 10544–10548.

Giannasca, P.J., and Neutra, M.R. (1993). Interactions of microorganisms with intestinal M cells: mucosal invasion and induction of secretory immunity. Infect. Agents Dis. *2*, 242–248.

Hapfelmeier, S., Ehrbar, K., Stecher, B., Barthel, M., Kremer, M., and Hardt, W.D. (2004). Role of the Salmonella pathogenicity island 1 effector proteins SipA, SopB, SopE, and SopE2 in Salmonella enterica subspecies 1 serovar Typhimurium colitis in streptomycin-pretreated mice. Infect. Immun. *72*, 795–809.

Hapfelmeier, S., Stecher, B., Barthel, M., Kremer, M., Müller, A.J., Heikenwalder, M., Stallmach, T., Hensel, M., Pfeffer, K., Akira, S., and Hardt, W.D. (2005). The Salmonella pathogenicity island (SPI)-2 and SPI-1 type III secretion systems allow Salmonella serovar typhimurium to trigger colitis via MyD88-dependent and MyD88-independent mechanisms. J. Immunol. *174*, 1675–1685.

Hapfelmeier, S., Müller, A.J., Stecher, B., Kaiser, P., Barthel, M., Endt, K., Eberhard, M., Robbiani, R., Jacobi, C.A., Heikenwalder, M., et al. (2008). Microbe sampling by mucosal dendritic cells is a discrete, MyD88-independent step in DeltainvG S. Typhimurium colitis. J. Exp. Med. *205*, 437–450.

Hase, K., Kawano, K., Nochi, T., Pontes, G.S., Fukuda, S., Ebisawa, M., Kadokura, K., Tobe, T., Fujimura, Y., Kawano, S., et al. (2009). Uptake through glycoprotein 2 of FimH(+) bacteria by M cells initiates mucosal immune response. Nature *462*, 226–230.

Hensel, M., Shea, J.E., Gleeson, C., Jones, M.D., Dalton, E., and Holden, D.W. (1995). Simultaneous identification of bacterial virulence genes by negative selection. Science *269*, 400–403.

Hoiseth, S.K., and Stocker, B.A. (1981). Aromatic-dependent *Salmonella typhimurium* are non-virulent and effective as live vaccines. Nature *291*, 238–239.

Huang, F.P., Platt, N., Wykes, M., Major, J.R., Powell, T.J., Jenkins, C.D., and MacPherson, G.G. (2000). A discrete subpopulation of dendritic cells transports apoptotic intestinal epithelial cells to T cell areas of mesenteric lymph nodes. J. Exp. Med. *191*, 435–444.

Hybiske, K., and Stephens, R.S. (2008). Exit strategies of intracellular pathogens. Nat. Rev. Microbiol. *6*, 99–110.

Jepson, M.A., Collares-Buzato, C.B., Clark, M.A., Hirst, B.H., and Simmons, N.L. (1995). Rapid disruption of epithelial barrier function by Salmonella typhimurium is associated with structural modification of intercellular junctions. Infect. Immun. *63*, 356–359.

Jones, B.D., Ghori, N., and Falkow, S. (1994). Salmonella typhimurium initiates murine infection by penetrating and destroying the specialized epithelial M cells of the Peyer's patches. J. Exp. Med. *180*, 15–23.

Jung, S., Aliberti, J., Graemmel, P., Sunshine, M.J., Kreutzberg, G.W., Sher, A., and Littman, D.R. (2000). Analysis of fractalkine receptor CX(3)CR1 function by targeted deletion and green fluorescent protein reporter gene insertion. Mol. Cell. Biol. *20*, 4106–4114.

Kaiser, P., Diard, M., Stecher, B., and Hardt, W.D. (2012). The streptomycin mouse model for Salmonella diarrhea: functional analysis of the microbiota, the pathogen's virulence factors, and the host's mucosal immune response. Immunol. Rev. *245*, 56–83.

Kaniga, K., Bossio, J.C., and Galán, J.E. (1994). The Salmonella typhimurium invasion genes invF and invG encode homologues of the AraC and PulD family of proteins. Mol. Microbiol. *13*, 555–568.

Kohbata, S., Yokoyama, H., and Yabuuchi, E. (1986). Cytopathogenic effect of Salmonella typhi GIFU 10007 on M cells of murine ileal Peyer's patches in ligated ileal loops: an ultrastructural study. Microbiol. Immunol. *30*, 1225–1237.

Köhler, H., Sakaguchi, T., Hurley, B.P., Kase, B.A., Reinecker, H.C., and McCormick, B.A. (2007). Salmonella enterica serovar Typhimurium regulates intercellular junction proteins and facilitates transepithelial neutrophil and bacterial passage. Am. J. Physiol. Gastrointest. Liver Physiol. *293*, G178–G187.

Macpherson, A.J., and Harris, N.L. (2004). Interactions between commensal intestinal bacteria and the immune system. Nat. Rev. Immunol. *4*, 478–485.

Magariyama, Y., Sugiyama, S., and Kudo, S. (2001). Bacterial swimming speed and rotation rate of bundled flagella. FEMS Microbiol. Lett. *199*, 125–129.

Meads, T., and Schroer, T.A. (1995). Polarity and nucleation of microtubules in polarized epithelial cells. Cell Motil. Cytoskeleton *32*, 273–288.

Müller, A.J., Hoffmann, C., Galle, M., Van Den Broeke, A., Heikenwalder, M., Falter, L., Misselwitz, B., Kremer, M., Beyaert, R., and Hardt, W.D. (2009). The S. Typhimurium effector SopE induces caspase-1 activation in stromal cells to initiate gut inflammation. Cell Host Microbe *6*, 125–136.

Niess, J.H., Brand, S., Gu, X., Landsman, L., Jung, S., McCormick, B.A., Vyas, J.M., Boes, M., Ploegh, H.L., Fox, J.G., et al. (2005). CX3CR1-mediated dendritic cell access to the intestinal lumen and bacterial clearance. Science *307*, 254–258.

Ramsden, A.E., Mota, L.J., Münter, S., Shorte, S.L., and Holden, D.W. (2007). The SPI-2 type III secretion system restricts motility of Salmonella-containing vacuoles. Cell. Microbiol. *9*, 2517–2529.

Reddy, E.A., Shaw, A.V., and Crump, J.A. (2010). Community-acquired bloodstream infections in Africa: a systematic review and meta-analysis. Lancet Infect. Dis. *10*, 417–432.

Reed, W.M., Olander, H.J., and Thacker, H.L. (1986). Studies on the pathogenesis of Salmonella typhimurium and Salmonella choleraesuis var kunzendorf infection in weanling pigs. Am. J. Vet. Res. *47*, 75–83.

Reilein, A., Yamada, S., and Nelson, W.J. (2005). Self-organization of an acentrosomal microtubule network at the basal cortex of polarized epithelial cells. J. Cell Biol. *171*, 845–855.

Reis, B.P., Zhang, S., Tsolis, R.M., Bäumler, A.J., Adams, L.G., and Santos, R.L. (2003). The attenuated sopB mutant of Salmonella enterica serovar Typhimurium has the same tissue distribution and host chemokine response as the wild type in bovine Peyer's patches. Vet. Microbiol. *97*, 269–277.

Santos, R.L., and Bäumler, A.J. (2004). Cell tropism of Salmonella enterica. Int. J. Med. Microbiol. *294*, 225–233.

Santos, R.L., Zhang, S., Tsolis, R.M., Bäumler, A.J., and Adams, L.G. (2002). Morphologic and molecular characterization of Salmonella typhimurium infection in neonatal calves. Vet. Pathol. *39*, 200–215.

Schlumberger, M.C., Käppeli, R., Wetter, M., Müller, A.J., Misselwitz, B., Dilling, S., Kremer, M., and Hardt, W.D. (2007). Two newly identified SipA domains (F1, F2) steer effector protein localization and contribute to Salmonella host cell manipulation. Mol. Microbiol. *65*, 741–760.

Schroeder, N., Mota, L.J., and Méresse, S. (2011). Salmonella-induced tubular networks. Trends Microbiol. *19*, 268–277.

Schulz, O., Jaensson, E., Persson, E.K., Liu, X., Worbs, T., Agace, W.W., and Pabst, O. (2009). Intestinal CD103+, but not CX3CR1+, antigen sampling cells

migrate in lymph and serve classical dendritic cell functions. J. Exp. Med. *206*, 3101–3114.

Stecher, B., and Hardt, W.D. (2011). Mechanisms controlling pathogen colonization of the gut. Curr. Opin. Microbiol. *14*, 82–91.

Stecher, B., Hapfelmeier, S., Müller, C., Kremer, M., Stallmach, T., and Hardt, W.D. (2004). Flagella and chemotaxis are required for efficient induction of Salmonella enterica serovar Typhimurium colitis in streptomycin-pretreated mice. Infect. Immun. *72*, 4138–4150.

Tafazoli, F., Magnusson, K.E., and Zheng, L. (2003). Disruption of epithelial barrier integrity by Salmonella enterica serovar typhimurium requires geranylgeranylated proteins. Infect. Immun. *71*, 872–881.

Takeuchi, A. (1967). Electron microscope studies of experimental *Salmonella* infection. I. Penetration into the intestinal epithelium by *Salmonella typhimurium*. Am. J. Pathol. *50*, 109–136.

Thevenaz, P., Ruttimann, U.E., and Unser, M. (1998). A pyramid approach to subpixel registration based on intensity. IEEE Transac on Image Proc. *7*, 27–41.

Tsolis, R.M., Adams, L.G., Ficht, T.A., and Bäumler, A.J. (1999). Contribution of *Salmonella typhimurium* virulence factors to diarrheal disease in calves. Infect. Immun. *67*, 4879–4885.

Turnbull, P.C., and Richmond, J.E. (1978). A model of salmonella enteritis: the behaviour of Salmonella enteritidis in chick intestine studies by light and electron microscopy. Br. J. Exp. Pathol. *59*, 64–75.

Vallon-Eberhard, A., Landsman, L., Yogev, N., Verrier, B., and Jung, S. (2006). Transepithelial pathogen uptake into the small intestinal lamina propria. J. Immunol. *176*, 2465–2469.

Varol, C., Vallon-Eberhard, A., Elinav, E., Aychek, T., Shapira, Y., Luche, H., Fehling, H.J., Hardt, W.D., Shakhar, G., and Jung, S. (2009). Intestinal lamina propria dendritic cell subsets have different origin and functions. Immunity *31*, 502–512.

Varol, C., Zigmond, E., and Jung, S. (2010). Securing the immune tightrope: mononuclear phagocytes in the intestinal lamina propria. Nat. Rev. Immunol. *10*, 415–426.

Vazquez-Torres, A., Jones-Carson, J., Bäumler, A.J., Falkow, S., Valdivia, R., Brown, W., Le, M., Berggren, R., Parks, W.T., and Fang, F.C. (1999). Extraintestinal dissemination of Salmonella by CD18-expressing phagocytes. Nature *401*, 804–808.

Wallis, T.S., Starkey, W.G., Stephen, J., Haddon, S.J., Osborne, M.P., and Candy, D.C. (1986). The nature and role of mucosal damage in relation to Salmonella typhimurium-induced fluid secretion in the rabbit ileum. J. Med. Microbiol. *22*, 39–49.

Watson, P.R., Paulin, S.M., Bland, A.P., Jones, P.W., and Wallis, T.S. (1995). Characterization of intestinal invasion by Salmonella typhimurium and Salmonella dublin and effect of a mutation in the invH gene. Infect. Immun. *63*, 2743–2754.

Watson, A.J., Chu, S., Sieck, L., Gerasimenko, O., Bullen, T., Campbell, F., McKenna, M., Rose, T., and Montrose, M.H. (2005). Epithelial barrier function in vivo is sustained despite gaps in epithelial layers. Gastroenterology *129*, 902–912.

Worley, M.J., Ching, K.H., and Heffron, F. (2000). *Salmonella* SsrB activates a global regulon of horizontally acquired genes. Mol. Microbiol. *36*, 749–761.